Available online at www.sciencedirect.com
SCIENCE DIRECT®
Journal of Computational Physics 203 (2005) 89–111
JOURNAL OF COMPUTATIONAL PHYSICS
www.elsevier.com/locate/jcp

# Lattice Boltzmann open boundaries for hydrodynamic models

A.F. Bennett [a,*], J.R. Taylor [b], B.S. Chua [a]

[a] College of Oceanic and Atmospheric Sciences, Oregon State University, COAS Admin. Bldg. 104, Corvallis 97331-5503, Oregon, USA
[b] Department of Mechanical and Aerospace Engineering, University of California, San Diego, La Jolla, California, USA

Received 22 January 2004; received in revised form 16 July 2004; accepted 9 August 2004
Available online 15 September 2004

**Abstract**

The mixed initial–boundary value problem for the equations of nonhydrostatic fluid dynamics is mathematically well posed, but is physically and computationally ill posed. The ill-posedness is exacerbated by boundary data taken from integrations of hydrostatic flow equations. The difficulty is found both in fully compressible flow and in Boussinesq flow; the latter is emphasized here. The mixed problem for the Boltzmann equation is well posed in every respect. Inserting lattice Boltzmann kinetics between hydrostatic boundary data and nonhydrostatic dynamics resolves the physical and computational ill-posedness of the dynamics, by relaxing the boundary data to nonhydrostatic dynamical consistency. Simple numerical experiments with boundary data taken from exact and approximate analytical solutions demonstrate the effectiveness of the approach.


*MSC:* 65M30; 76M28; 86A05; 86A10
*Keywords:* Open boundaries; Ill-posedness; Lattice Boltzmann

## 1. Introduction

It is ironic that the introduction of digital computing into fluid dynamics has produced a new 'classical' problem for partial differential equations: the initial value problem in a limited region, or region with open boundaries. The practical experience in numerical weather prediction and in ocean hindcasting is that the solutions are highly sensitive to errors in boundary: see [1–6] and their references. This sensitivity is to be expected when the boundary data are generated by a numerical model with a larger domain, different numerical resolution or a different numerical method. For example, phase speeds of gravity waves in fully

* Corresponding author. Tel.: +1 541 737 9352; fax: +1 541 737 8681.
*E-mail address:* bennett@coas.oregonstate.edu (A.F. Bennett).

0021-9991/$ - see front matter © 2004 Elsevier Inc. All rights reserved.
doi:10.1016/j.jcp.2004.08.007

spectral global models do not suffer from horizontal truncation, while those in finite difference models have well known errors [7, p. 115].

However, it was unexpected that Oliger and Sundström [8] would be able to prove that the initial value problem with open boundaries (or *mixed* problem) for inviscid, nonconducting hydrostatic dynamics is classically ill posed. They show, even after linearizing about a horizontally uniform and steady stable stratification, and about a uniform constant horizontal wind field, that it is impossible to choose satisfactory spatially and temporally local boundary conditions on vertical boundaries (that is, on boundaries that are vertical). In general, choices of such 'vertical boundary conditions' lead either to discontinuous solutions or to undetermined solutions. There may be fortuitous choices of boundary values that yield continuity, such as values obtained by perfect measurement of the ideal fluid being modeled. The argument of Oliger and Sundström involves separating the flow into vertical internal modes which have amplitudes propagating horizontally as gravity waves in shallow water. The waves have phase speeds $c_n = \mathrm{O}(n^{-1})$, where $n$ is the order of the internal mode. The number and type of boundary conditions required by each mode depends upon the magnitude and sign of the internal Froude number $U/c_n$, where $U$ is the component of the fluid velocity normal to the boundary. There would be no difficulty if the dynamics were integrated mode by mode, but that is as a rule impractical owing to varying stratification, orography, etc.

The finding of Oliger and Sundström are rejected in [9], where it is shown to be possible to choose local conditions on vertical boundaries in such a way that the ideal, nonlinear hydrostatic dynamics lead to well defined analytical continuation off the boundaries. Assuming the existence of a nonzero radius of convergence, [9], in effect establishes existence of solutions in neighbourhoods of the vertical boundaries. Yet the investigation in [9] is incomplete, since classical well-posedness also requires that the solution be uniquely and continuously dependent upon the prescribed boundary values. Uniqueness and continuous dependence may be addressed by considering the dynamics of finite-amplitude flow disturbances. Oliger and Sundström showed that even the linearized dynamics of disturbances do not lead to well posed problems, given local boundary conditions.

It may be shown [10,11] that the generalized inverse problem for the linearized, ideal hydrostatic equations is mathematically well posed in open regions. That is, there is a unique solution to the Euler–Lagrange equations for the best fit to any interior data, to the dynamics, to the initial conditions, and to local boundary values for both horizontal components of the fluid velocity and for the pressure. The fit is defined by weighted squares, summed over the domain and over the 'smoothing' time interval of interest. It may also be shown [12] that the forward integration problem is well posed if the open boundary consists of moving fluid particles of fixed identity, that is, if the open boundary is *comoving*, since the local Froude number vanishes in the comoving reference frame. Alas, we must for many applications continue to integrate forward in fixed open regions. In particular, efficient variational data assimilation requires forward and backward integrations, either to calculate the gradient of the penalty functional in state space, or to solve the Euler–Lagrange equations which hold when the gradient vanishes. Both the forward and backward problems for the Primitive Equations are ill posed, and there is no partitioning of the boundary conditions in the Euler–Lagrange equations which overcomes this difficulty, even though the Euler–Lagrange system is well posed as a boundary value problem in space *and* time.

Practical numerical weather prediction (NWP) models include parameterizations of subgridscale processes. These are often expressed simply in terms of eddy viscosities, eddy conductivities and eddy diffusivities in general. The parabolic operators for rates of change owing to divergences of diffusive fluxes dominate the dynamics mathematically, even if the diffusivities are small. It is therefore intuitively obvious that advection and gravity wave propagation are not issues when choosing boundary conditions, and a simple choice of local boundary conditions yields a well posed problem. However, it is remarked in [13] that "the addition of viscous or diffusive terms can give rise to spurious boundary layers that may propagate, interact and contaminate the flow elsewhere". [13] continues: "it would be better to use the more complete set of (nonhydrostatic) Euler equations, rather than the hydrostatic primitive ones, in order to put the for-

mulation of a regional model on a sounder theoretical footing''. Indeed, oceanographers are developing nonhydrostatic models of regional circulation: see [14] for a description of a nonhydrostatic Boussinesq model of the general ocean circulation. Fully compressible regional nonhydrostatic NWP models are now in operation, e.g. [15]. The Euler equations include nonhydrostatic accelerations, in particular the horizontal advection of vertical momentum, and so intuitively the equations require at least the specification of vertical velocity at vertical boundaries.

The emergence of spurious boundary layers in diffusive hydrostatic dynamics may be demonstrated with a simple 'toy' model that is readily solved with analytical methods. The same toy model also demonstrates that, while nondiffusive nonhydrostatic dynamics can yield mathematically well posed problems, the spurious advecting boundary layers are replaced by spurious packets of nonhydrostatic internal gravity waves which would cause as much trouble for computation and interpretation. Thus, while the inclusion of nonhydrostatic effects does render the nondiffusive problem mathematically well posed, it remains computationally and physically ill posed. The toy model and the analytical solution are available at an anonymous ftp site. [1]

In spite of the penetrating analysis of Oliger and Sundström, choices of boundary conditions remain strongly influenced by earlier approaches [16,17]. The influence is especially strong in NWP. Both these approaches involve blending the time rates of change of prescribed boundary values with the rates of change provided by the dynamics in the immediate interior. All prognostic variables are so treated, regardless of the sign or the magnitude of the local Froude number.

It is argued here that the mathematical ill-posedness of the mixed initial-boundary value problem for the hydrostatic Primitive Equations, and the computational and physical ill-posedness of the nonhydrostatic equations, may be resolved by replacing conventional computational fluid dynamics with Lattice Boltzmann or 'LB' models consistent with nonhydrostatic fluid dynamics. The mixed problems for LB models are mathematically, computationally and physically well posed. It is assumed that practioners of regional modeling would not want to abandon conventional finite difference ('FD') models which have been so long in development. Hence the approach advocated and tested here is the insertion of an intermediate region between an outer region (the domain for a hydrostatic FD model), and an inner region (the domain of a nonhydrostatic FD model). The intermediate region or 'moat' is the domain of an LB model, which can accept hydrostatic solutions at the outer boundary, relax them to nonhydrostatic solutions and pass these across the inner boundary. The ill-posedness of the inner model is ameliorated by passing it boundary data which are physically reasonable extrapolations of the outer hydrostatic solution, and which are exactly compatible with the inner nonhydrostatic dynamics. The LB model receives nonhydrostatic boundary data at the inner boundary from the inner FD model, that is, nesting at the inner boundary is necessarily 'two way'.

Simple LB models consistent with fully compressible flow are as yet unsatisfactory for two reasons: first, they tend to be unstable for realistic ranges of the Mach number and Froude number; second, the solutions are contaminated with unrealistic sound waves. The first problem may be solved by the introduction of two-distribution LB models. The second may solved by requiring that the LB model be consistent only with the dynamics of a Boussinesq fluid [18]. Both steps have been taken here. As a consequence of the Boussinesq approximation, these first results are more applicable to ocean modeling than to NWP. An anelastic LB model may suffice for NWP.

The outline of this paper is as follows: the continuous Boltzmann equation is introduced in Section 2, where it is shown that mixed initial boundary value problems are well posed. The boundary condition aside, the material in this section is classical physics [19], but is not well known to many computational fluid dynamicists and so is included to facilitate the subsequent discussion. Equally, the many

[1] ftp.coas.oregonstate.edu/dist/bennett/LB/toy.pdf

details related to implementation on a lattice are mostly standard; they are summarized in Section 3, and given in full in Appendices A, B, C, D, E. Finite-amplitude, plane-wave analytical solutions of the fluid dynamical equations, given in detail in Appendix E, are used in Section 4 to test LB and FD solutions in the vertical plane. Nesting experiments are reported in Section 5. These are summarized and conclusions are drawn in Section 6.

## 2. Boltzmann's equation

The difficulties with regional boundaries can be resolved by the use of Lattice-Boltzmann techniques. The essence of the approach is most simply explained with the continuous Boltzmann equation. The lattice approximation may then be introduced as a discrete analog. In gas dynamics, the velocity $u_j$ ($j = 1,2,3$) is a vector field which depends upon position $x_k$ ($k = 1,2,3$) and time $t$. In gas kinetics, the vector $v_j$ at $(x_k,t)$ is an independent variable with unbounded range. It is a possible value for the velocity of one of many gas molecule close to that point, at that time. The value is idealised as a random variable with a distribution function $N(v_j,x_k,t)$ satisfying Boltzmann's equation, e.g. [19,20]

$$\frac{\partial N}{\partial t} + \sum_j v_j \frac{\partial N}{\partial x_j} = J, \tag{2.1}$$

where $J$ consists of terms binary in $N$, integrated over one of the pair of velocity–vector arguments. This 'collision operator' represents changes in $N$ owing to collisions at $(x_k,t)$ between pairs of gas molecules. It is assumed that the collisions conserve mass, momentum and energy, that is

$$\int\int\int \left(1, v_k, \sum_j v_j^2\right) J \, \mathrm{d}v_1 \, \mathrm{d}v_2 \, \mathrm{d}v_3 = (0,0,0) \tag{2.2}$$

for monatomic gas molecules without internal degrees of freedom. The distribution function is normalized so that

$$m \int\int\int N(v_1, v_2, v_3, x_j, t) \, \mathrm{d}v_1 \, \mathrm{d}v_2 \, \mathrm{d}v_3 = \rho(x_j, t), \tag{2.3}$$

where $m$ is the mass of a gas molecule, and $\rho$ is the thermodynamic or macroscopic or fluid density of the gas. [The shortcomings of subscript notation are evident in (2.3). The alternative is boldface for vectors, which leads to boldface sans serif for tensors and dyads: the result is impenetrable.] The fluid velocity $u_j$ is then given by

$$\rho u_j(x_k, t) = m \int\int\int v_j N(v_1, v_2, v_3, x_k, t) \, \mathrm{d}v_1 \, \mathrm{d}v_2 \, \mathrm{d}v_3, \tag{2.4}$$

while the fluid stress tensor is given by

$$\Pi_{ij}(x_k, t) = m \int\int\int v_i v_j N(v_1, v_2, v_3, x_k, t) \, \mathrm{d}v_1 \, \mathrm{d}v_2 \, \mathrm{d}v_3. \tag{2.5}$$

The distribution $N$ is isotropic if

$$\Pi_{ij} = \rho u_i u_j + p\delta_{ij}, \tag{2.6}$$

where $p$ will be identified with the fluid pressure; $\delta_{ij}$ is the Kronecker delta.

Detailed examination shows that the binary collision term $J$ vanishes if $N$ is the isotropic Maxwell–Boltzmann equilibrium distribution

$$N_{\mathrm{eq}} = \frac{\rho}{m}\left(\frac{2\pi p}{\rho}\right)^{-3/2} \exp\left(-\frac{\rho}{2p}\sum_j (v_j - u_j)^2\right). \tag{2.7}$$

If the flow is uniform, that is, if $\rho$, $u_j$ and $p$ are independent of position and time, then $N_{\mathrm{eq}} = N_{\mathrm{eq}}(v_j;\rho,u_j,p)$ is clearly an exact solution of (2.1). Boltzmann's $H$-theorem guarantees that for gases which are initially uniform in space, $N$ must relax towards $N_{\mathrm{eq}}$ as $t \to \infty$ (see e.g. [19]). In all but the most rarified nonuniform flow, the time and distance between molecular collisions are far smaller than the time and space scales of the flow. Hence the equilibrium distribution $N_{\mathrm{eq}}$ satisfies (2.1) very closely, even in nonuniform flow. There are exceptional regions, for example very close to a rigid wall, where the tangential velocity of each molecule is that of the wall.

Let us return to the general case of nonequilibrium velocity distributions $N$. Multiplying (2.1) by the molecular mass $m$ and integrating over velocity yields the conservation of fluid mass

$$\frac{\partial \rho}{\partial t} + \sum_j \frac{\partial}{\partial x_j}(\rho u_j) = 0. \tag{2.8}$$

Multiplying (2.1) by the molecular momentum $mv_i$ and integrating yields the conservation of fluid momentum

$$\rho\left(\frac{\partial u_i}{\partial t} + \sum_k u_k \frac{\partial u_i}{\partial x_k}\right) = -\frac{\partial p}{\partial x_i}, \tag{2.9}$$

assuming that $N$ that is isotropic. Multiplying (2.1) by the molecular kinetic energy $\frac{1}{2}m\sum v_j^2$ and integrating yields the conservation of fluid energy

$$\frac{\partial p}{\partial t} + \sum_j u_j \frac{\partial p}{\partial x_j} = \gamma \frac{p}{\rho}\left(\frac{\partial \rho}{\partial t} + \sum_j u_j \frac{\partial \rho}{\partial x_j}\right), \tag{2.10}$$

again assuming isotropy of $N$, where $\gamma = (d+2)/d$ for a monatomic gas without internal degrees of freedom, in $d$ space dimensions. Recall that for an ideal gas, $\gamma p/\rho = \gamma RT = c_s^2$ is the square of the speed sound. Again, isotropy of $N$ has been assumed. Detailed derivation of moment equations from (2.1) for weakly anisotropic distributions leads to the Navier–Stokes equations [19]. In particular, there are divergences of Newtonian shear and bulk stresses in the generalization of (2.9), and both mechanical dissipation and divergences of Fourier heat fluxes in the generalization of (2.10). There can be no diffusion of mass in (2.8), by definition of the density $\rho$ and the momentum flux $\rho u_j$.

The selection of boundary conditions for (2.1) at open boundaries is trivial, regardless of the isotropy or anisotropy of $N$. The velocity distribution function $N$ should be specified for incoming molecules, but should not be specified for outgoing molecules. If only the thermodynamical fields $\rho$, $u_j$ and $p$ were known at the boundary at $(x_k,t)$, then the natural choice for $N$ at the boundary would be the isotropic equilibrium distribution

$$N(v_j;x_k,t) = N_{\mathrm{eq}}(v_j;\rho,u_j,p) \text{ if } \sum_i v_i n_i < 0, \tag{2.11}$$

where $n_i$ is the outward normal on the boundary. It is natural, therefore, that all the fluid variables $\rho$, $u_j$, $p$ be specified on the entire boundary so that the right hand side of (2.11) can be evaluated. Note that the Maxwell–Boltzmann equilibrium distribution (2.7) is uniquely determined by the fluid variables. This much information would certainly overspecify the fluid-dynamical initial-boundary value problem, and spurious boundary layers and spurious packets of internal waves should be expected. The fluid variables are moments of the velocity distribution $N$, so it too might be expected to be misbehaved. However, (2.11) does

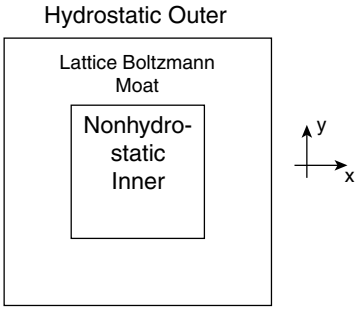


Fig. 1. Boltzmann 'moat' around an open region containing a fluid.

not impose values of $\rho$, $u_j$, or $p$ on the boundary. If values of $N$ are given only for incoming molecules, then only partial moments can be evaluated, such as

$$\rho^{\mathrm{IN}} \equiv m \int\int\int_{\mathrm{IN}} N \, \mathrm{d}v_1 \, \mathrm{d}v_2 \, \mathrm{d}v_3 \tag{2.12}$$

with analogous definitions for $u_j^{\mathrm{IN}}$ and $p^{\mathrm{IN}}$. The complementary part

$$\rho^{\mathrm{OUT}} \equiv m \int\int\int_{\mathrm{OUT}} N \, \mathrm{d}v_1 \, \mathrm{d}v_2 \, \mathrm{d}v_3 \tag{2.13}$$

is not being imposed on the Boltzmann Eq. (2.1) as boundary information. Adopting the convention that the molecules with velocities tangential to the boundary are included in OUT, that is, $\sum_i v_i n_i \geqslant 0$, then (2.11) partitions the boundary data for density as

$$\rho = \rho^{\mathrm{IN}} + \rho^{\mathrm{OUT}} \tag{2.14}$$

and similarly for $u_j$ and $p$, in a way which is consistent with the detailed molecular kinematics. Discontinuities can develop, but only within the domain, and only in the form of shocks owing to convergence of the fluid continuum.

Within the domain, the moments of the anisotropic distribution $N$ will be exactly compatible with the Navier–Stokes equations. The moments will be approximately compatible with the Euler Eqs. (2.8)–(2.10), and closely so for suitably chosen relaxation coefficients in the collision operator $J$. Thus, values of $\rho$, $u_j$ and $p$ obtained as moments of $N$ would be almost exactly compatible as boundary data for a fluid dynamical model in a region interior to the first inner region. That is, a Boltzmann 'moat' around an open Euler interior or open Navier–Stokes interior would be the most natural way to relax boundary data provided by smoothed and imperfect observations, or by a less accurate model of the exterior fluid dynamics: see Fig. 1. It might be somewhat more informative about the 'LB moat' to refer to the condition (2.11) at the outer boundary of the moat as a 'coupling condition'; in the interest of minimal jargon we shall simply use the strictly correct if less specific term 'boundary condition'.

## 3. Implementation

### 3.1. Lattice Boltzmann equation

It is not necessary, for the purposes of simulating hydrodynamics, to solve Boltzmann's equation for a continous distribution of molecular velocities $v_k$ in the range $-\infty < v_k < \infty$. It suffices to consider a discrete

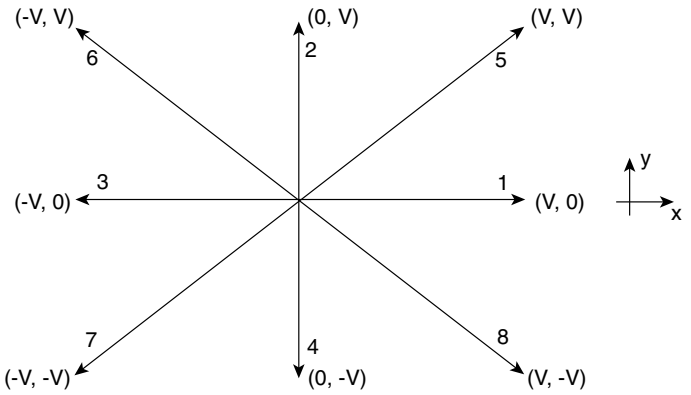


Fig. 2. Planar lattice with nine velocities, including (0,0).

and finite set of velocities $v_k^q$, for $0 \leqslant q \leqslant Q$, defined by transitions on a spatial lattice: see Fig. 2. There is correspondingly a discrete set of probabilities $N^q$, for $0 \leqslant 1 \leqslant Q$ at each lattice vertex and at each time $t$. Fluid density, momentum and stress are defined as moments with respect to the discrete distribution, and a Lattice Boltzmann equation is readily defined in terms of finite differences: see Appendix A. The Lattice Boltzmann equation was first used for ocean modeling in [21], where may be found an especially insightful analysis of the equation and its fluid dynamical limit. It may be shown [22] that there is a lattice equilibrium distribution $N^q_{\mathrm{eq}}$ which annihilates the binary collision sum $J^q$ analogous to the binary collision operator $J$ in (2.1). This lattice equilibrium distribution is, like (2.7), uniquely determined by the fluid variables $\rho$, $u_i$, $p$.

### 3.2. BGK approximation

The parameters in the 'Lattice-Maxwell Boltzmann' distribution $N^q_{\mathrm{eq}}$ devised in [22,23] are not explicitly related to the fluid variables $\rho$, $u_j$ and $p$. Hence, numerical tuning of the parameters over a usefully wide range of the variables is extremely difficult [24]. In particular, given values of the flow variables at a boundary, it is very difficult to construct the corresponding discrete equilibrium distribution. The 'collision-interval theory' advocated by Bhatnagar et al. [25] approximates binary collision operators by

$$J^q = -\frac{1}{\tau}(N^q - N^q_{\mathrm{eq}}). \tag{3.1}$$

Subject to this collision term, $N^q$ will relax towards $N^q_{\mathrm{eq}}$ over the time scale $\tau$. Detailed analysis, e.g. [26], shows that as a result of the inhomogeneity of the flow, the departures from equilibrium will be anisotropic. These assumptions lead to kinematic shear viscosities and kinematic conductivities proportional to $V^2(\tau - \Delta t/2)$. The great advantage of (3.1) is that any convenient functional form may be used for $N^q_{\mathrm{eq}}$. There are explicitly tunable polynomials, see e.g. [27], which are uniquely determinded by $\rho$, $u_i$, $p$. The polynomials are at least quadratic in the fluid fields, which are in turn moments of $N^q$, so the seemingly linear expression (3.1) is actually nonlinear in $N^q$. As a result, the BGK lattice Boltzmann equation for compressible flow is unstable in general; see [28].

### 3.3. Two-distribution planar LB

It has been found by experimentation [29,30] that the instability of 'BGK LB' for stratified flow may be avoided by introducing a second distribution. In the case of two-dimensional flow simulated on the

9-velocity lattice shown in Fig. 2, the second distribution is of the form $M^q$, for $0 \leqslant q \leqslant Q = 8$. This second distribution also satisfies a BGK LB equation. The two equilibrium distributions $N^q_{\rm eq}, M^q_{\rm eq}$ may be chosen so that the moments of their BGK LB equations yield the Navier–Stokes equations for compressible flow: see Appendix B. It may be remarked that an 18-velocity lattice is required if the planar, compressible Navier–Stokes equations are to be recovered from a single-distribution LB equation [31].

### 3.4. Boussinesq approximation

Sound waves are not an important mechanism for dynamical adjustment of circulation in either the atmosphere or ocean. However the Mach number in the stratosphere is not very small, so there is little computational advantage to filtering out sound waves. That is, the numerical stability criterion for explicit time stepping schemes is not significantly relaxed by excluding such waves. Also, pressure is the preferred vertical coordinate for analyzing meteorological fields, and the equation of conservation of mass is easily integrated in pressure coordinates [7]. In the ocean, on the other hand, the Mach number is extremely small. Also, the equation of conservation of volume is easily integrated if the vertical coordinate is simply the depth. Thus it is of great advantage to exclude sound waves by imposing the Boussinesq approximation [18]. A slight variant of the two-velocity LB model of a Boussinesq fluid given by [30] is employed here: see Appendix C. It should be remarked that the molecular precursors to spurious sound waves can be troublesome on a Boltzmann lattice, and so the LB method favors a Boussinesq fluid.

### 3.5. Simple wave solutions

Assume a spatially uniform and temporally constant mean horizontal fluid velocity $U$, a stable static density profile $\overline{\rho}(z)$ and hydrostatically-balanced pressure $\overline{p}(z)$. Ignore the vertical variation in these thermodynamic variables as they appear as coefficients in the fluid dynamical equations. Then disturbances in the vertical velocity of the form

$$w = W \sin(\kappa x + \omega t) \sin(\lambda z) \tag{3.2}$$

and similarly for the other fluid variables, constitute exact solutions. In (3.2), $\kappa = 2\pi/L$, where $L$ is the wavelength in the unbounded horizontal direction, $\lambda = 2\pi/H$ where $H$ is the vertical distance between rigid walls, and $\omega = 2\pi/S$ where $S$ is the period. The dispersion relation between $\omega$, $\kappa$ and $\lambda$ involves both $U$ and the Nyquist frequency $\mathcal{N}_0$ for internal waves: see Appendix D. The dynamic pressure $p^{\rm dyn}$ includes exact quadratic corrections to the simple wave form related to (3.2). These finite-amplitude solutions provide convenient and reasonably representative tests for the BGK LB model.

## 4. Tests of 2D Boussinesq LB

The finite-amplitude, simple-wave analytical solution given in Appendix D for a stably-stratified Boussinesq fluid, together with the conventional finite difference solutions of the 2D form of the Boussinesq equations given in Appendix C, provide tests for the two-distribution compressible LB model given in Appendix B and modified for Boussinesq flow in Appendix C. The numerical method and the fluid dynamical boundary conditions are described in Appendix E. In particular, the flow fields in the equilibrium distributions at the boundaries are provided by the analytical solutions.

The amplitude of the wave solution is characterized by the Froude number $Fr$ defined by

$$Fr = \frac{W^2\kappa^2}{\mathcal{N}_0^2}, \tag{4.2}$$

which is a dimensionless measure of the fluid kinetic energy $W^2$, in a wave motion having horizontal wavenumber $\kappa$. The horizontal phase speed is $O(\mathcal{N}_0/\kappa)$, in the absence of a mean horizontal velocity: see the dispersion relation (D.16); assume $U = 0$, and $\kappa = O(\lambda)$.

In the first experiment, the initial conditions are the velocity $(u,w)$ and dynamic density $\rho^{dyn}$ for the simple wave (D.5)–(D.13). The case is $\alpha = 1$ (nonhydrostatic), $\beta = 0$ (Boussinesq). The boundary conditions are taken from the same solution, which is exact for all $Fr$. The boundary values for dynamic pressure $p^{dyn}$ are corrected as in (D.18), and so are also taken from an exact solution.

Shown in Fig. 3 are: {solid lines} the analytical solution (AN) of the inviscid, nonconducting, nonhydrostatic Boussinesq equations ($Fr = 0.7$); {dashed lines} the tenfold amplified error in the finite-difference (FD) solution, that is, $10 \times (\mathrm{FD} - \mathrm{AN})$ ; and {dotted lines} the tenfold amplified error in the LB solution, that is, $10 \times (\mathrm{LB} - \mathrm{AN})$. The agreement amongst the three solutions is remarkable, even after 5 periods. The three solutions AN, FD and LB are practically indistinguishable when plotted in full. With periodic boundary conditions (not shown), the LB solution decays several percent per cycle. The decay rate is determined by the relaxation time $\tau$ in (B.1) and in (B.14). Note again that the kinematic viscosity and conductivity implicit in these 9-velocity LB models are $O(V^2(\tau - \Delta t/2))$, where $V = \Delta x/\Delta t$ is the molecular speed on the space-time lattice. In these experiments, $\tau = 0.5001\Delta t$; the simple stability requirement is clearly $\tau > 0.5\Delta t$. The choice of relaxation time $\tau$ is empirical; the onset of nonlinear instability for BGK LB simulation of stratified flow is Froude number dependent, being less stable at higher Froude number. The value $Fr = 0.7$ in the following experiments is appropriate for the most intense circulations in the Gulf Stream, and far larger than appropriate for the atmospheric jet stream. For further discussion of LB stability, see e.g. [26,28]. See Table 1 for all the parameters used in these experiments.

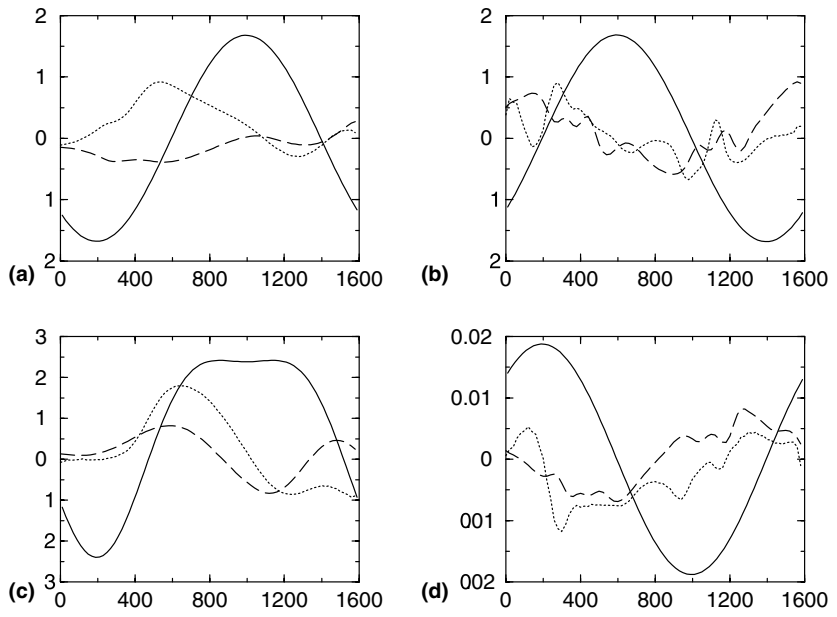


Fig. 3. {Solid lines}: single-wave, finite-amplitude analytical solution analytical solution (AN) of the nonhydrostatic Boussinesq equations ($Fr = 0.7$). {Dashed lines}: tenfold amplified error in integrations of a finite-difference (FD) model with nonhydrostatic initial and boundary data from AN, after 5 periods, that is, $10 \times (\mathrm{FD} - \mathrm{AN})$. {Dotted lines}: tenfold amplified error in a Lattice-Boltzmann model (LB), that is, $10 \times (\mathrm{LB} - \mathrm{AN})$. Panels: (a) $u$ m/s vs. $x$ m at $z = H/2$ m; (b) $w$ m/s vs. $x$ at $z = H/4$; (c) $p^{dyn}$ Pa vs. $x$ at $z = H/2$; (d) $\rho^{dyn}$ kg/m$^3$ vs. $x$ at $z = H/4$.

Table 1

| |
|---|
| *The domain and the LB grid* |
| $L = 1600$ m, $H = 1600$ m |
| $\Delta x = 20$ m, $\Delta z = 20$ m, $\Delta t = 0.025$ s |
| $\tau = 0.5001\Delta t$, $V = 800$ m s$^{-1}$ |
| *The mean stratification* |
| $\overline{\rho}_0 = 1.0$ kg m$^{-3}$, $c_s = 462$ m s$^{-1}$ |
| $(\mathrm{d}\overline{\rho}/\mathrm{d}z)_0 = -6.25 \times 10^{-4}$ kg m$^{-4}$, $g = 1.0$ m s$^{-2}$ |
| $\mathcal{N}_0 = 7.91 \times 10^{-3}$ s$^{-1}$, $U = 0$ m s$^{-1}$ |
| *The plane waves* |
| $\omega = -5.59 \times 10^{-3}$ s$^{-1}$, $W_1 = 1.684$ m s$^{-1}$, $W_2 = 0.5$ m s$^{-1}$ |
| $\kappa_1 = (2\pi/L)$ m$^{-1}$, $\kappa_2 = 3\kappa_1$ |
| $\lambda_1 = (2\pi/H)$ m$^{-1}$, $\lambda_2 = \lambda_1$ |
| $Fr = 0.7$ (based on Wave #1) |

The initial conditions and boundary conditions for the second experiment are the same as those in the first, but their values are taken from a sum of two simple waves (denoted with subscripts 1 and 2 in Table 1). The LB, FD and analytical solutions agree closely for $Fr = .0089$ (not shown). The entire FD solution {dashed line}, and entire LB solution {dotted line}, after a half period, are shown in Fig. 4 for $Fr = 0.7$. The analytical solution is unknown. The integration of the FD model cannot be extended beyond a half period since the boundary data are not taken from an analytical solution. The data are therefore not compatible with the nonhydrostatic dynamics, and so the *physical* ill-posedness of the nonhydrostatic mixed problem leads to very badly-behaved solutions exhibiting packets of short-wavelength, high-frequency nonhydro-

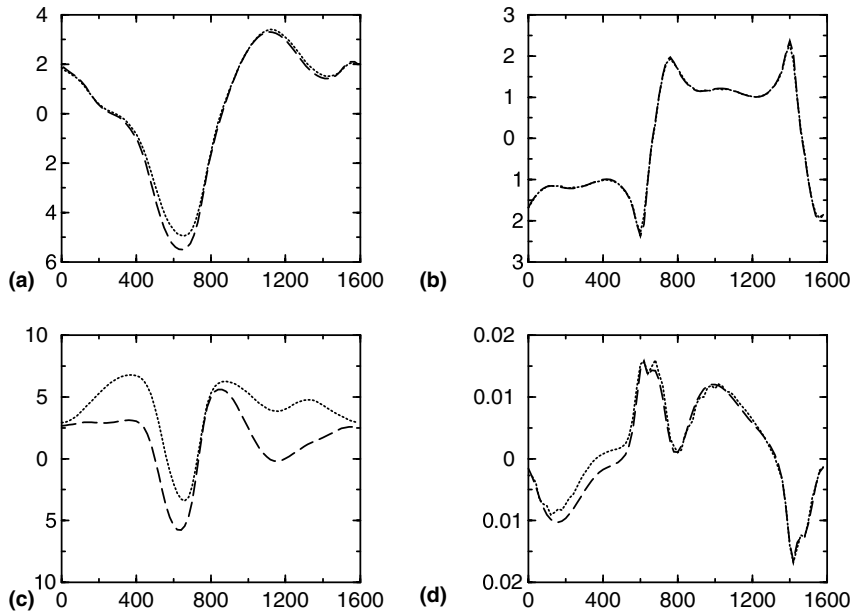


Fig. 4. Integrations as in Fig. 3 {FD dashed, LB dotted}, but with periodic boundary conditions, and with initial conditions from a two-wave field that is an approximate solution only for small Froude number. Here, $Fr = 0.7$ and the integrations are only for half a period. The analytical field is not known. (a) $u$; (b) $w$; (c) $p^{\mathrm{dyn}}$; (d)$\rho^{\mathrm{dyn}}$; all at levels as in Fig. 3.

static internal gravity waves. For the first half-period, however, the agreement between LB and FD is remarkably good except for pressure. It is not known which numerical solution is the more accurate. Pressure, velocity and density are all moments of the LB equations, but whereas velocity and density are solutions of the fluid mechanical moment equations (Euler equations for momentum and energy), pressure is diagnosed effectively through the incompressibility condition. It is concluded from these experiments that the LB model is as accurate as the FD model at approximating incompressible, nonhydrostatic internal gravity waves of large amplitude.

## 5. Nesting experiments

The method of nesting which will be explored here incorporates a LB 'moat' separating an outer region from an inner region. The outer is the domain of an hydrostatic model, the inner is the domain of a nonhydrostatic model. In general the two models will have different resolution, and may even have quite different numerics. As there is only one horizontal dimension here, the LB moat is in two disconnected parts: see Fig. 5. Again, the function of the moats is to relax the hydrostatic data at the outer boundaries towards nonhydrostatic consistency at the inner boundaries. The three contiguous segments are each of the same size as the single domain in the preceding tests (1600 m × 1600 m), but the spatial resolution is twice as coarse: (40 m × 40 m), and the time step is much coarser (0.4 s). All other parameters are the same as in the preceding tests: see Table 1.

In these experiments, the role of the outer hydrostatic model (for example, the US Navy Operational Global Atmospheric Prediction System or 'NOGAPS'; see http://www.fnmoc.navy.mil/PUBLIC/) is taken by analytical expressions. Specifically, the boundary data needed by the LB model in the moat are taken from the nonhydrostatic and hydrostatic single-wave analytical solutions ($Fr = 0.7$), rather than integrations of an outer model. The LB model, which implies nonhydrostatic flow, requires the distributions $N^q$ and $M^q$ for molecular inflow, that is, inflow values of $v^q$. These values are taken from the equilibrium distributions $N^q_{\mathrm{eq}}$, $M^q_{\mathrm{eq}}$, which are in turn determined by the dynamic density $\rho^{\mathrm{dyn}}$, fluid velocity $\mathbf{u}$ and dynamic pressure $p^{\mathrm{dyn}}$: see (C.4) and (C.7). The values of all these fields must therefore be provided to the LB model at the outer boundaries of the two-piece moat. The outer nesting here is 'one way', that is, the LB solution has no influence on the outer solution. The LB model also requires inflow distributions at the inner boundary. These are again provided by the inflow equilibrium distributions, but the moments $\rho^{\mathrm{dyn}}$, $\mathbf{u}$ and $p^{\mathrm{dyn}}$ are provided by the nonhydrostatic model in the inner region (representing the US Navy Coupled Ocean/Atmosphere Mesoscale Prediction System or 'COAMPS', for example; see http://www.fnmoc.navy.mil/PUBLIC/). The horizontal grids for the LB moat and the nonhydrostatic interior overlap by one interval: see Fig. 6, which shows the nodes near the left inner boundary at $x = 1600$ m (which is the right boundary of the left moat). The rightmost open circle (LB index $i = nx$) indicate the innermost node of the moat

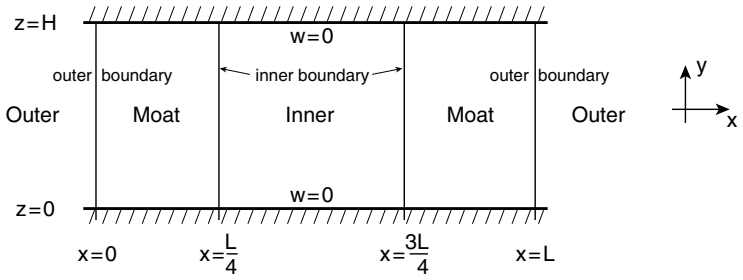


Fig. 5. Two-part Boltzmann moat separating a one-dimensional inner nonhydrostatic region from an outer hydrostatic region.

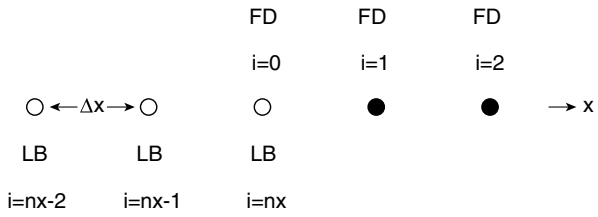


Fig. 6. {Open circles}: adjacent nodes of the Boltzmann lattice. {Solid circles}: the fluid finite-difference grid.

at which an LB collision takes place; the leftmost filled circle (FD index $i = 1$) indicates the outermost node at which the FD model is timestepped. Where necessary, LB moments on the LB grid are determined from FD fields on the staggered FD grid by simple interpolation. Finally, note that inflow equilibrium distributions with hydrostatic moments are specified at LB index $i = 1$ and streamed, with collisions, to LB index $i = nx$. The moments relax to nonhydrostatic dynamical consistency as a consequence of those LB 'collisions'.

Physical boundary conditions for the FD model at FD index $i = 0$ in the inner region are provided by the LB solution. Dynamic density, dynamic pressure at fluid inflow (where $u$ is flowing in), and vertical velocity $w$ at inflow are computed from the moments of the LB solutions. That is, nesting at the inner boundary is 'two way'. Where necessary, fluid variables on the staggered FD grid are determined from LB moments on the LB grid by simple interpolation.

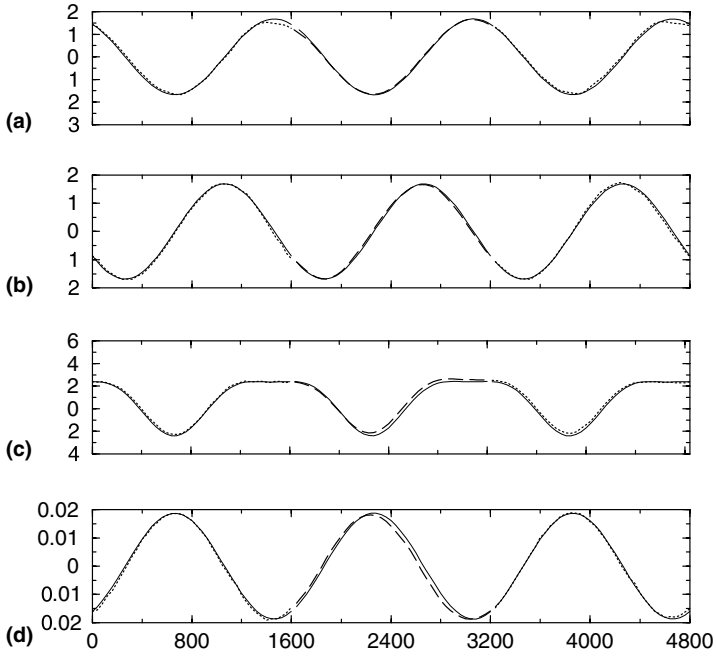


Fig. 7. {Dotted lines}: LB solution in left ($0 \leqslant x \leqslant 1600$ m) and right ($3200 \leqslant x \leqslant 4800$ m) segments of the outer 'moat', subject to nonhydrostatic boundary data at $x = 0$ m and at $x = 4800$ m. {Dashed line}: FD solution in the inner region ($1600 \leqslant x \leqslant 3200$ m), with two-way nesting at $x = 1600$ m and at $x = 3200$ m; nonhydrostatic initial data everywhere. The boundary and initial data are taken from a single-wave nonhydrostatic exact analytical solution for $Fr = 0.7$ {thin solid line}: (a) $u$; (b) $w$; (c) $p^{\mathrm{dyn}}$; (d) $\rho^{\mathrm{dyn}}$.

Initial conditions for the FD and LB integrations in the moat and inner region are provided by the *nonhydrostatic* single-wave analytical solution.

The analytical solution for $Fr = 0.7$ {thin solid line}, the entire FD solution {heavy dashed line}, and the entire LB solutions {dotted lines} are shown in Fig. 7, after two periods. In this experiment there *is* an analytical solution, as the outer boundary data are taken from the same *nonhydrostatic* single-wave analytical solution as the initial data. The LB and FD solutions are in excellent agreement with the analytical solution in their respective domains. Plotting the amplified errors in this complicated nesting configuration is in some respects clearer, but overall is too confusing. Shown in Fig. 8 are the results of an integration, again for two periods, with outer boundary data for the relaxing LB moats taken from the *hydrostatic* single-wave analytical solution. There is now no analytical solution in either the nonhydrostatic LB domains or in the nonhydrostatic FD domain. The hydrostatic analytical solution given hydrostatic outer data and initial conditions is shown {thin dashed line}, as is the nonhydrostatic analytical solution {thin solid line} with the same initial vertical velocity as the hydrostatic analytical solution. Also shown in the FD region is a numerical integration {heavy solid line} with inner boundary data taken from the hydrostatic analytical solution but *nonhydrostatic* initial conditions. This will be referred to as the unrelaxed FD integration, in distinction to the previously described integrations relaxed by LB moats. It resembles operational practice in numerical weather prediction:

1. In the inner or FD domain (1600 m $\leqslant x \leqslant$ 3200 m), the unrelaxed integration {heavy solid line} not only fails to resemble either analytical solution, but lacks any credibility owing to the rapid formation of strong gradients not present in the initial data nor in the inner boundary data at $x = 1600$, 3200 m. The smooth behaviour of the data are manifest in the hydrostatic solution {thin dashed line}.

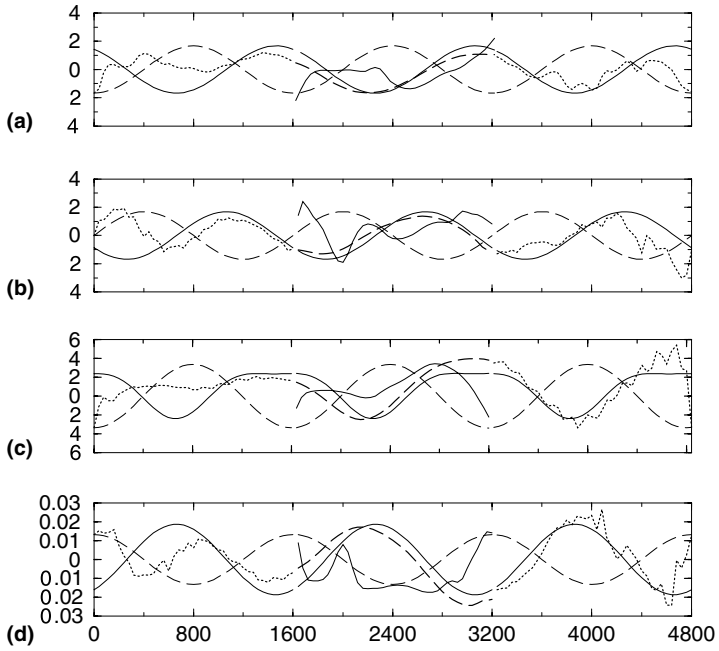


Fig. 8. As for Fig. 7, except boundary data at $x = 0$, 4800 m are taken from a {thin dashed line} single-wave hydrostatic analytical solution . {Thin solid line}: the nonhydrostatic analytical solution, with the same initial vertical velocity as the hydrostatic analytical solution. {Thick solid line}: the FD solution, subject to hydrostatic boundary data at $x = 1600$, 3200 m.

2. In the inner or FD domain, the integration {heavy dashed line joining dotted lines} subject to boundary data relaxed by moats is as smooth as the initial and boundary data, and reasonably resembles the nonhydrostatic analytical solution {thin solid line} even though the outer boundary data at $x = 0$, 4800 m are hydrostatic.
3. The success of the FD integration owes to the relaxation of the LB solutions towards the nonhydrostatic solution, as kinetic information propagates away from the outer boundaries and towards the inner boundaries.

## 6. Summary

It has been shown, by comparison with finite-amplitude analytical solutions for internal gravity waves, that the insertion of a Lattice Boltzmann 'moat' between hydrostatic fluid dynamics in an outer region and nonhydrostatic dynamic in an inner region has promise for resolving the physical and computational ill-posedness of the mixed initial–boundary value problem. The LB approach is in principle applicable to compressible flow, but Boussinesq flow has been emphasized here. The success of these experiments depends critically upon the effectiveness of a two-distribution LB model at overcoming instabilities associated with single-distribution thermodynamic LB models. The success may not be universal, but the stability issue is the subject of much research at present. See [32] for a recent review, including a concise tour of the statistical–mechanical background.

Reliable arithmetic concerning the computational cost of a three-dimensional moat cannot yet be provided. Consider an inner region with square plan form. Append a moat of the same shape and size as the inner region to each of the four vertical faces of the latter, for a fourfold expansion of volume and computation. This is a huge cost, even though it excludes the four 'corners' of the connected moat shown in Fig. 1. Yet in their seminal 1986 study of regional weather forecasting, Robert and Yakimiw [1] argue for an expansion of the plan forms of limited regions by even greater factors, with corners included, in order to postpone the impact of boundary noise upon the central forecast region. We speculate that the existence of two transverse directions for collisions in a three dimensional moat would accelerate relaxation, and thus moats as wide as the inner region should not be necessary. On the other hand, the principal goal of this study is to find the first rational solution to the longstanding and vexed problem of the ill-posedness of regional computational fluid dynamics. Efficiency is not the first concern. That said, the pursuit of efficiency should, as already mentioned, address the width of the moat. Again, the exploration of the geometrical parameter space should be conducted with a three dimensional model. The 'diagonal' BGK collision operator (3.1) employed here could be replaced with a nondiagonal operator having a range of eigenvalues [33], with further potential not only for simulating a range of Prandtl numbers, but also for accelerating the relaxation process in the moat. In addition, nondiagonal operators permit the simulation of complex constitutive relations such as nonisotropic viscosity and viscoelasticity, for insignificant computational cost.

The LB approach needs also to be demonstrated for compressible flow. Sound waves and lattice waves can be a nuisance when integrating Lattice Boltzmann equations, but an anelastic LB moat should suffice for the nesting of flows at low Mach number. Furthermore, the inner FD model should be subject to radiation conditions rather than the adiabatic conditions 1–5 of Appendix E: see [12].

It may well be more effective in the long run to abandon the inner, nonhydrostatic fluid dynamical model entirely, in favor of a LB model driven at its open boundaries by equilibrium distribution values for incoming molecular velocities. Indeed, it has recently been argued in [34] that extended Boltzmann kinetics are more efficient than fluid dynamics at modeling turbulent flow in general.

It has been candidly stated [35] by a leading advocate of the Lattice Boltzmann method that there is as yet no 'compelling application' which justifies the method over all others. We submit that the resolution of the mixed problem in computational fluid dynamics is just such an application.

**Acknowledgements**

Much of this work was carried out while A.F.B. and J.R.T. were supported by the Visiting Scientist Program of the University Corporation for Atmospheric Research, and were located at the Office of Naval Research Science Unit, Fleet Numerical Meteorology and Oceanography Center, Monterey CA. It is a great pleasure to acknowledge the hospitality and the productive environment provided by Captain Joseph Swaykos USN and his entire staff at 'Fleet Numerical'. Continuation of the work is being supported by NSF award OCE-0121542. The constructive comments by the reviewers are greatly appreciated. We were introduced to Lattice Boltzmann techniques by Julia Muccino.

## Appendix A. The Lattice Boltzmann equation

Boltzmann's equation determines the evolution, in continuous space and time, of the distribution $N$ of molecular velocities which lie in the range $-\infty < v_j < \infty$ ($j = 1,2,3$). Such detail is not needed for a numerical 'moat'. It suffices to determine the distribution at each vertex of a fine, regular lattice in space and time. The 'molecules' need only be capable of occupying vertices, and jumping to neighbouring vertices in a fixed time interval. Thus, only a finite set of molecular velocities need be admitted.

An example of a planar lattice is shown in Fig. 2. The nine admitted velocities are:

$$(0,0),(V,0),(0,V),(-V,0),(0,-V),(V,V),(-V,V),(-V,-V),(V,-V), \tag{A.1}$$

which shall be denoted $v_j^q$, $0 \leqslant q \leqslant Q$, where $Q = 8$ here.

The value of $V$ is uniquely $\Delta x/\Delta t$ where $\Delta x$ and $\Delta t$ are the lattice intervals. It is assumed that the lattice is square: $\Delta x_1 = \Delta x_2 = \Delta x$. The real-valued velocity distribution function $N(v_j; x_k, t)$ is replaced at each vertex by $Q + 1$ real numbers $N^q(x_k, t), 0 \leqslant q \leqslant Q$. The flow variables are defined at each vertex value of $(x_k,t)$ by:

$$\rho(x_k,t) = m\sum_{q=0}^{Q} N^q(x_k,t), \tag{A.2}$$

$$\rho u_j(x_k,t) = m\sum_{q=1}^{Q} v_j^q N^q(x_k,t), \tag{A.3}$$

$$\Pi_{ij}(x_k,t) = m\sum_{q=1}^{Q} v_i^q v_j^q N^q(x_k,t). \tag{A.4}$$

An example of a Lattice Boltzmann equation for the $N^q$ is

$$N^q(x_k + v_k^q\Delta t, t + \Delta t) = N^q(x_k,t) + \Delta t J^q, \tag{A.5}$$

where $J^q$ is a collision operator. A Taylor series expansion of (A.5) yields (2.1), to leading order. The collision operator may be defined as a binary product of the $N^q$ summed over one of the pair of velocity vectors [22,23], such that the collisions conserve mass, momentum and energy. The sum has an equilibrium distribution $N_{\mathrm{eq}}^q$ for which $J^q$ vanishes, and so (A.5) is exactly satisfied by uniform gases in equilibrium. There is even [22] an $H$-theorem for the lattice collision operator. See the reviews [36,37] for further details of the LB method.

The selection of boundary conditions for (A.5) at open boundaries is again trivial, regardless of the isotropy or anisotropy of $N^q$. The values $N^q$ should be specified for incoming molecules, but should not be specified for outgoing molecules. If only the thermodynamical fields $\rho$, $u_j$ and $p$ are known at the boundary at $(x_k,t)$, then the natural choice for 'inflow' at the boundary would be the isotropic equilibrium distribution

$$N^q = N^q_{\text{eq}} \text{ if } \sum_i v^q_i n_i < 0. \tag{A.6}$$

It is assumed that the lattice equilibrium distribution depends, like the Maxwell–Boltzmann distribution (2.7), only upon the fluid density, momentum and pressure. Then the values of $N^q_{\text{eq}}$ for the prescribed $\rho$, $u_j$ and $p$ may be determined by satisfaction of (A.2)–(A.4), after noting that $\Pi^{\text{eq}}_{ij} = \rho u_i u_j + p\delta_{ij}$ since $N^q_{\text{eq}}$ is isotropic on the lattice. Again, (A.6) partitions the fluid data at the boundary into additive IN and OUT components, with only the IN component influencing the interior flow. Examples of lattice equilibrium distributions $N^q_{\text{eq}}$ depending only upon $\rho$, $u_j$ and $p$ are given below.

## Appendix B. Two-distribution planar LB: compressible fluid

The first of the two LB equations is the combination of (A.5) and (3.1)

$$N^q(x_k + v^q_k \Delta t, t + \Delta t) = N^q(x_k, t) - \frac{\Delta t}{\tau}(N^q - N^q_{\text{eq}}). \tag{B.1}$$

The fluid density and fluid momentum $\rho$ and $\rho u_k$ are again defined to be the normalizing and first moments $N^q$, as in (A.2) and (A.3), respectively. Then conservation of mass (2.8) is an identity, within truncation error. The ideal conservation of momentum (2.9) is correct to leading order, for distributions $N^q$ close to isotropic equilibria $N^q_{\text{eq}}$ such as in [27]:

$$N^q_{\text{eq}} = \frac{w_q \rho}{m}\left[1 + \frac{3\mathbf{v}^q \cdot \mathbf{u}}{V^2} + \frac{9(\mathbf{v}^q \cdot \mathbf{u})^2}{2V^4} - \frac{3|\mathbf{u}|^2}{2V^2}\right], \tag{B.2}$$

where

$$w_0 = \tfrac{4}{9}, \quad w_{1,2,3,4} = \tfrac{1}{9}, \quad w_{5,6,7,8} = \tfrac{1}{36}, \tag{B.3}$$

and

$$\mathbf{v}^q \cdot \mathbf{u} = \sum_k v^q_k u_k. \tag{B.4}$$

Note that (A.2)–(A.4) hold also for $N^q_{\text{eq}}$. Pressure is not an independent parameter in (B.2), but is related to density by

$$p = \tfrac{1}{3}\rho V^2. \tag{B.5}$$

Hence the speed of sound $c_s$ is related to the lattice speed by

$$c_s = \frac{V}{\sqrt{3}}, \tag{B.6}$$

rather than obeying the ideal gas relation

$$c_s = \sqrt{\frac{\gamma p}{\rho}} \tag{B.7}$$

with $\gamma = 2$ in two dimensions ($\gamma = 5/3$ in three dimensions). Buoyancy is introduced by the addition of a source term to (B.1):

$$N^q(x_k + v_k^q \Delta t, t + \Delta t) = N^q(x_k, t) - \frac{\Delta t}{\tau}(N^q - N_{\mathrm{eq}}^q) - \frac{\Delta t g \rho^{\mathrm{dyn}} v_K^q}{6V^2}, \tag{B.8}$$

where the vertical index $K$ equals $d$ (the number of dimensions: $d = 2$ or 3), $g$ is the gravitational acceleration and $\rho^{\mathrm{dyn}} = \rho - \overline{\rho}$, where $\overline{\rho} = \overline{\rho}(z)$ is a static density distribution. The pressure obtained from the second moment of $N^q$ is the dynamic pressure $p^{\mathrm{dyn}} = p - \overline{p}$, where $\overline{p}$ and $\overline{\rho}$ are in hydrostatic balance. The normalizing and first moment Eqs. (2.8) and (2.9) are unaltered except for the vertical momentum balance, which now incorporates the buoyancy force:

$$\rho\left(\frac{\partial u_K}{\partial t} + \sum_j u_j \frac{\partial u_K}{\partial x_j}\right) = -\frac{\partial p^{\mathrm{dyn}}}{\partial x_K} - g\rho^{\mathrm{dyn}}. \tag{B.9}$$

However, it would be thermodynamically incorrect to calculate the buoyancy using the normalizing moment of $N^q$. Even if $N^q \approx N_{\mathrm{eq}}^q$, the latter distribution implies the thermodynamically incorrect sound speed (B.6). Again, single-distribution 18-velocity LB-BGK models may be constructed which are thermodynamically correct [31], but these are unstable. Now the energy-conservation Eq. (2.10) and mass-conservation Eq. (2.8) imply

$$\frac{\partial p}{\partial t} + \sum_j u_j \frac{\partial p}{\partial x_j} = -\gamma p \sum_k \frac{\partial u_k}{\partial x_k}. \tag{B.10}$$

For an ideal gas

$$p = R\rho T \tag{B.11}$$

or

$$p = 2\rho\varepsilon d^{-1}, \tag{B.12}$$

where $d$ is the spatial dimension and $\varepsilon$ is the internal energy per unit mass. Hence (B.10) and (2.8) imply that

$$\frac{\partial \varepsilon}{\partial t} + \sum_j \frac{\partial}{\partial x_j}(u_j \varepsilon) = -(\gamma - 2)\varepsilon \sum_k \frac{\partial u_k}{\partial x_k}. \tag{B.13}$$

Consider first the case of two space dimensions: $d = 2$, $\gamma = 2$. The right hand side of (B.13) vanishes, and the equation takes the same form as (2.8) with $\varepsilon$ replacing $\rho$. This suggests introducing a second 9-velocity distribution $M^q$ satisfying a second LB equation

$$M^q(x_k + v_k^q \Delta t, t + \Delta t) = M^q(x_k, t) - \frac{\Delta t}{\tau}(M^q - M_{\mathrm{eq}}^q), \tag{B.14}$$

where the equilibrium distribution is simply

$$M_{\mathrm{eq}}^q = w_q \varepsilon\left[1 + \frac{3\mathbf{v}^q \cdot \mathbf{u}}{V^2}\right] \tag{B.15}$$

with $w_q$ defined as in (B.3). The fluid velocity $u_j$ is still defined as a the first moment of $N^q$ as in (A.2), but the internal energy per unit mass is defined as the normalizing moment of $M^q$

$$\varepsilon = \sum_q M^q. \tag{B.16}$$

If $M^q \approx M^q_{\mathrm{eq}}$, then

$$\sum_q v^q_k M^q \approx u_k \varepsilon \tag{B.17}$$

and so (B.13) is recovered. The internal energy having been computed using (B.14)–(B.16), buoyancy is recovered as

$$-g\rho^{\mathrm{dyn}} = -g\left(\frac{dp}{2\varepsilon} - \overline{\rho}\right), \tag{B.18}$$

which is, with sufficient accuracy in shallow convection

$$-g\rho^{\mathrm{dyn}} \cong -g\overline{\rho}\left(\frac{p^{\mathrm{dyn}}}{\overline{p}} - \frac{\varepsilon^{\mathrm{dyn}}}{\overline{\varepsilon}}\right) \cong g\overline{\rho}\frac{\varepsilon^{\mathrm{dyn}}}{\overline{\varepsilon}}, \tag{B.19}$$

where $\overline{\varepsilon} = d\overline{p}/2\overline{\rho}$.

For 3D flow, $\gamma = 5/3$ and so the right hand side of (B.13) does not vanish. It may be introduced into (B.14) as a source. The two-distribution, 9-velocity LB model has only limited ability to represent compressible stratified flow, owing to the lattice equation of state (B.5). By implication, the hydrostatic density profile must be

$$\overline{p}(z) = \overline{p}(0)\exp[-z\zeta^{-1}], \tag{B.20}$$

where the scale height $\zeta$ is

$$\zeta = c_s^2 g^{-1} = \tfrac{1}{3}V^2 g^{-1}. \tag{B.21}$$

That is, the two-distribution, 9-velocity LB model can only represent an isothermal atmosphere with the constant, static, absolute temperature $\overline{T} = (3\gamma R)^{-1}V^2$. The inner and outer fluid dynamical models do not in general assume isothermal atmospheres, so some dynamical adjustment would be instigated by the use of the isothermal equilibrium distributions. Many operational forecasting models already make various assumptions about static stratifications at various stages in their solution algorithms, so 100% thermodynamic purity would not be lost by the use of isothermal equilibria in the LB moat. The two-distribution, 6-velocity hexagonal LB model in [30] permits arbitrary equations of state.

## Appendix C. Two distribution planar LB: Boussinesq fluid

The equations of motion for a shallow Boussinesq fluid are [18]:

$$\overline{\rho}_0\left(\frac{\partial u_j}{\partial t} + \sum_k u_k\frac{\partial u_j}{\partial x_k}\right) = -\frac{\partial p^{\mathrm{dyn}}}{\partial x_j} - g\rho^{\mathrm{dyn}}\delta_{jK}, \tag{C.1}$$

$$\sum_j \frac{\partial u_j}{\partial x_j} = 0, \tag{C.2}$$

$$\frac{\partial \rho^{\mathrm{dyn}}}{\partial t} + \sum_k u_k\frac{\partial \rho^{\mathrm{dyn}}}{\partial x_k} + u_K\frac{\mathrm{d}\overline{\rho}}{\mathrm{d}x_K} = 0. \tag{C.3}$$

Note that the sound speed $c_s$ does not appear in these equations. It is pointed out in [29] that (C.1) and (C.2) may be recovered, with sufficient accuracy, as the first moment and the normalizing moment of (B.8), respectively, provided that the equilibrium distribution (B.2) is replaced with

$$N^q_{\rm eq} = \frac{w_q \overline{\rho}_0}{m}\left[\frac{3p^{\rm dyn}}{\overline{\rho}_0 V^2} + \frac{3\mathbf{v}^q\cdot\mathbf{u}}{V^2} + \frac{9(\mathbf{v}^q\cdot\mathbf{u})^2}{2V^4} - \frac{3|\mathbf{u}|^2}{2V^2}\right]. \tag{C.4}$$

Assuming that $N^q \approx N^q_{\rm eq}$, and taking the normalizing moment of (B.8) leads to

$$c_{\rm s}^{-2}\frac{\partial p^{\rm dyn}}{\partial t} + \overline{\rho}_0 \sum_k \frac{\partial u_k}{\partial x_k} = 0, \tag{C.5}$$

where $c_{\rm s}^2 = V^2/3$. Taking the first moments leads to (C.1). Thus the lattice supports sound waves having speed $c_{\rm s} = V/\sqrt{3}$, but their amplitude is small if the initial flow divergence vanishes. The relative error in (C.5), as an approximate representation of the Boussinesq continuity Eq. (C.2), is of order $\mu^2$ where $\mu = |\mathbf{u}|/c_{\rm s}$ is the Mach number. The dynamic density $\rho^{\rm dyn}$ is determined as the normalizing moment of the second distribution $M^q$, which satisfies

$$M^q(x_k + v^q_k\Delta t, t+\Delta t) = M^q(x_k,t) - \frac{\Delta t}{\tau}(M^q - M^q_{\rm eq}) - \frac{\Delta t u_K}{Q+1}\frac{{\rm d}\overline{\rho}}{{\rm d}x_K} \tag{C.6}$$

with $M^q_{\rm eq}$ given by

$$M^q_{\rm eq} = w_q \rho^{\rm dyn}\left[1 + \frac{3\mathbf{v}^q\cdot\mathbf{u}}{V^2}\right]. \tag{C.7}$$

The normalizing moment of (C.6) is, with error of order $\mu^2$, the Boussinesq energy Eq. (C.3).

## Appendix D. Finite-amplitude waves

Specializing to 2D flow, and adopting the notation $(x_1,x_2) = (x,z)$, $(u_1,u_2) = (u,w)$, etc., consider a constant uniform fluid velocity $(u,w) = (U,0)$, a density profile $\overline{\rho} = \overline{\rho}(z)$ and a hydrostatic pressure profile $\overline{p} = \overline{p}(z)$, where ${\rm d}\overline{p}/{\rm d}z = -g\overline{\rho}$. Linearized, constant-coefficient Euler equations for compressible flow are:

$$\frac{\partial \rho^{\rm dyn}}{\partial t} + U\frac{\partial \rho^{\rm dyn}}{\partial x} + w\left(\frac{{\rm d}\overline{\rho}}{{\rm d}z}\right)_0 + \overline{\rho}_0\left(\frac{\partial u}{\partial x} + \frac{\partial w}{\partial z}\right) = 0, \tag{D.1}$$

$$\overline{\rho}_0\left(\frac{\partial u}{\partial t} + U\frac{\partial u}{\partial x}\right) = -\frac{\partial p^{\rm dyn}}{\partial x}, \tag{D.2}$$

$$\alpha\overline{\rho}_0\left(\frac{\partial w}{\partial t} + U\frac{\partial w}{\partial x}\right) = -\frac{\partial p^{\rm dyn}}{\partial z} - g\rho^{\rm dyn} \tag{D.3}$$

and

$$\frac{\partial \rho^{\rm dyn}}{\partial t} + U\frac{\partial \rho^{\rm dyn}}{\partial x} + w\left(\frac{{\rm d}\overline{\rho}}{{\rm d}z}\right)_0 = \frac{\beta}{c_0^2}\left(\frac{\partial p^{\rm dyn}}{\partial t} + U\frac{\partial p^{\rm dyn}}{\partial x} + \left(w\frac{{\rm d}\overline{p}}{{\rm d}z}\right)_0\right), \tag{D.4}$$

where $c_0^2 = \gamma\overline{p}_0/\overline{\rho}_0$. Note that the flow is nonhydrostatic or hydrostatic according to $\alpha = 1$ or 0, and is compressible or shallow-Boussinesq according to $\beta = 1$ or 0. Had the Euler Eqs. (D.1)–(D.4) been nondimensionalized, $\alpha$ would be the Froude number while $\beta$ would have been the square of the Mach number. The zero subscript on the thermodynamic variables refers to a reference state, such as at $z = 0$. Assume that the flow is confined between rigid horizontal plates: $w = 0$ at $z = 0$, $H$; that the flow is periodic in the horizontal with wavelength $L$, and is also periodic in time with period $S$. A simple solution of (D.1)–(D.4) is

$$w = W\sin\theta\sin\lambda z, \tag{D.5}$$

where $\theta = \kappa x + \omega t$, $\kappa = 2\pi/L$, $\lambda = 2\pi/H$ and $\omega = 2\pi/S$

$$p^{\mathrm{dyn}} = \Pi(z)\cos\theta, \tag{D.6}$$

where

$$\Pi(z) = a\sin(\lambda z) + b\cos(\lambda z), \tag{D.7}$$

$$a = \frac{\beta F\chi}{\chi^2\lambda^2 + \beta^2}, \quad b = -\frac{\lambda F\chi^2}{\chi^2\lambda^2 + \beta^2}, \tag{D.8}$$

where $\chi \equiv c_0^2 g^{-1}$ is the scale height of the stratification, while:

$$F = \frac{W\overline{\rho}_0}{\omega + \kappa U}\left[\mathscr{N}_0^2 - \frac{g\beta}{\chi} - \alpha(\omega + \kappa U)^2\right], \tag{D.9}$$

$$u = -\frac{\kappa\cos\theta\Pi}{\overline{\rho}_0(\omega + \kappa U)} \tag{D.10}$$

and

$$\rho^{\mathrm{dyn}} = -\frac{\cos\theta}{g}\frac{\mathrm{d}\Pi}{\mathrm{d}z} - \frac{\alpha\overline{\rho}_0}{g}(\omega + \kappa U)W\cos\theta\sin(\lambda z). \tag{D.11}$$

In (D.9), $\mathscr{N}_0$ is the Nyquist frequency given by

$$\mathscr{N}_0^2 = -g\left(\frac{1}{\overline{\rho}}\frac{\mathrm{d}\overline{\rho}}{\mathrm{d}z}\right)_0. \tag{D.12}$$

The wave frequency $\omega$ must satisfy the dispersion relation

$$\alpha\beta(\omega + \kappa U)^4 - (\omega + \kappa U)^2[\beta\mathscr{N}_0^2 + c_0^2(\alpha\kappa^2 + \lambda^2)] + (c_0^2 N_0^2 - \beta g^2)\kappa^2 = 0. \tag{D.13}$$

If the flow is compressible ($\beta = 1$) there are two sound-wave branches; for large sound speed ($c_0\kappa N_0^{-1} \to \infty$), their asymptotes are:

$$\omega \sim -\kappa U \pm c_0\sqrt{\alpha\kappa^2 + \lambda^2}. \tag{D.14}$$

Regardless of the value of $\beta$, there are always two gravity-wave branches. Their large sound-speed asymptotes are:

$$\omega \sim -\kappa U \pm \frac{\mathscr{N}_0\kappa}{\sqrt{\alpha\kappa^2 + \lambda^2}}. \tag{D.15}$$

The analysis of Oliger and Sundström [8] is based upon (D.15). If the flow is hydrostatic ($\alpha = 0$), then

$$\omega \sim \kappa\left(-U \pm \frac{\mathscr{N}_0}{\lambda}\right) \tag{D.16}$$

and so signals can propagate upstream if and only if the flow is subcritical: $|U| < \mathscr{N}_0\lambda^{-1}$. Hence the number of conditions that need to be imposed at an open boundary depends upon the vertical wavenumber. This precludes the specification of model boundary conditions level-by-level. If the flow is nonhydrostatic ($\alpha = 1$), then for large sound speed and large horizontal wavenumber $\kappa \gg \mathscr{N}_0|U|^{-1}$, the asymptotic dispersion relation for the gravity wave branch is

$$\omega \sim -\kappa U \pm \mathscr{N}_0 \tag{D.17}$$

and so all signals are swept downstream. No boundary conditions are needed at outflow, and the number needed at inflow is the same for all vertical modes. Hence the inflow model boundary conditions maybe specified level-by-level.

The analytical expressions (D.5), (D.10) and (D.11) for $w$, $u$ and $\rho^{\mathrm{dyn}}$ are in fact exact solutions of the finite-amplitude Eqs. (C.1)–(C.3), but the expression (D.6) for $p^{\mathrm{dyn}}$ is not. The reason is that advection of vorticity and advection of dynamic density both vanish identically, but the divergence of momentum advection does not. With the addition of the pressure correction

$$p^{\mathrm{corr}} = \frac{\rho_0 W^2}{4}\cos(2\lambda z) - \frac{\rho_0 \lambda^2 W^2}{4\kappa^2}\cos(2\theta), \tag{D.18}$$

an exact solution is obtained for the dynamic pressure $p^{\mathrm{dyn}}$.

A more challenging test field is provided by a sum of two such simple waves having different amplitudes $W$ and wavenumbers $(\kappa,\lambda)$, without any pressure correction. The sum is not an exact solution of the finite amplitude equations, but is approximately so when the field has small amplitude.

## Appendix E. Solving the fluid dynamics

The Boussinesq equations are readily solved numerically by

1. diagnosing for the dynamic pressure $p^{\mathrm{dyn}}$ with the Poisson equation

$$\nabla^2 p^{\mathrm{dyn}} = -\bar{\rho}_0\left(\left(\frac{\partial u}{\partial x}\right)^2 + 2\frac{\partial u}{\partial z}\frac{\partial w}{\partial x} + \left(\frac{\partial w}{\partial z}\right)^2\right) - g\frac{\partial \rho^{\mathrm{dyn}}}{\partial z}, \tag{E.1}$$

2. predicting the vertical velocity $w$ with the vertical component of (C.1),
3. predicting the dynamic density $\rho^{\mathrm{dyn}}$ with (C.3) and
4. predicting the horizontal velocity $u$ with the horizontal component of (C.1).

The following boundary information suffices:

1. $p_z^{\mathrm{dyn}}$ (=$-g\rho^{\mathrm{dyn}}$: see 5. below) at $z = 0$, $H$ for all $x$;
2. $p^{\mathrm{dyn}}$ at $x = 0$, $L$ for all $z$;
3. the *sign* of $u$ at $x = 0$, $L$ for all $z$;
4. $w$ and $\rho$ on fluid inflow, at $x = 0$, $L$ for all $z$;
5. $w$ (=0) at $z = 0$, $H$ for all $x$.

These boundary conditions may be inferred from the low Mach-number limit of the boundary conditions for compressible flow. The latter conditions may be deduced using standard energy arguments, as in the classic intermediate text [38, Chapter VI, Section 3, p. 656]. The special case of compressible flow is developed in detail in [8]. No boundary condition for the *magnitude* of $u$ is needed at either $x = 0$ or $x = L$, since the normal advection of $u$ may be eliminated using (C.2). Initial conditions for $u$, $w$ and $\rho$ are prescribed by analytical solutions based on one or two waves.

The spatial finite difference scheme is based on the Arakawa C grid [39]. The time stepping scheme is first order forward, for both velocity components and for density. The pressure gradients and the Laplacian of pressure are second order centered. The Poisson equation is solved with the subroutine HWSCRT [40]. The advection scheme is 'QUICK' [41].

The two distributions $N^q$ and $M^q$ for the LB model are readily stepped in time using the BGK LB equations (B.8) and Eq. (B.14), respectively. Initial conditions are prescribed by the equilibrium distributions (C.4) and (C.7), respectively, with the analytical solution for the flow fields. The rigid boundary conditions at $z = 0$, $H$ are readily imposed using simple free-slip 'bounce-back' conditions, see e.g. [35]. At the open boundaries at $x = 0$, $L$, the LB distributions are prescribed for inflowing molecules only: see (2.11), with an analogous condition for $M^q$. The flow fields in the equilibrium distributions at the boundaries are prescribed by the analytical solutions.

The parameters in the experiments reported in Section 4 are listed in Table 1.

## References

[1] A. Robert, E. Yakimiw, Identification and elimination of an inflow computational boundary solution in limited area model integrations, Atmos. Ocean. 24 (1986) 369.
[2] T.T. Warner, R.A. Paterson, R.E. Treadon, A tutorial on lateral boundary conditions as a basic and potentially serious limitation to regional numerical weather prediction, Bull. Am. Met. Soc. 78 (1997) 2599.
[3] E.D. Palma, R.P. Matano, On the implementation of passive open boundary conditions to a general circulation model, J. Geophys. Res. 103 (1998) 1319.
[4] R.L. Greatbatch, G.L. Mellor, An overview of coastal ocean models, Coast. Estuarine Stud. 56 (1999) 31.
[5] A. McDonald, A step toward transparent boundary conditions for meteorological models, Mon. Weather Rev. 130 (2002) 140.
[6] A. McDonald, Testing transparent boundary conditions for the shallow water equations in a nested environment, HIRLAM Technical Report 54, SMHI, S-601 76 Norrkoping, Sweden, 2002.
[7] G.J. Haltiner, R.T. Williams, Numerical Prediction and Dynamical Meteorology, second ed., Wiley, New York, 1980.
[8] J. Oliger, A. Sundström, Theoretical and practical aspects of some initial boundary value problems in fluid dynamics, SIAM J. Appl. Math. 35 (1978) 419.
[9] J. Norbury, M.P. Cullen, A note on the properties of the primitive hydrostatic equations of motion, Quart. J. Roy. Met. Soc. 111 (1985) 1135.
[10] A.F. Bennett, Inverse Methods in Physical Oceanography, Cambridge University Press, Cambridge, UK, 1992.
[11] A.F. Bennett, B.S. Chua, Open-ocean modeling as an inverse problem: the primitive equations, Mon. Weather Rev. 122 (1994) 1326.
[12] A.F. Bennett, B.S. Chua, Open boundary conditions for Lagrangian geophysical fluid dynamics, J. Comput. Phys. 153 (1999) 418.
[13] A. Staniforth, Regional modelling: a theoretical discussion, Meteorol. Atmos. Phys. 63 (1997) 15.
[14] J. Marshall, A. Adcroft, C. Hill, L. Pereleman, C. Heisey, A finite-volume, incompressible Navier–Stokes model for studies of the ocean on parallel computers, J. Geophys. Res. 102 (1997) 5753.
[15] R. Hodur, The Naval Research Laboratory's Coupled Ocean/Atmosphere Mesoscale Prediction System (COAMPS), Mon. Weather Rev. 125 (1997) 1414.
[16] H.C. Davies, A lateral boundary formulation for multi-level prediction models, Quart. J. Roy. Meteor. Soc. 102 (1976) 405.
[17] D.J. Perkey, C.W. Kreitzberg, A time-dependent lateral boundary scheme for limited-area primitive equation models, Mon. Weather Rev. 104 (1976) 744.
[18] O.M. Phillips, The Dynamics of the Upper Ocean, Cambridge University Press, Cambridge, UK, 1966.
[19] S. Chapman, T.G. Cowling, The Mathematical Theory of Nonuniform Gases, third ed., Cambridge University Press, Cambridge, UK, 1970.
[20] C.J. Thompson, Mathematical Statistical Mechanics, Princeton University Press, Princeton, 1972.
[21] R. Salmon, The lattice Boltzmann method as a basis for ocean circulation modeling, J. Mar. Res. 57 (1999) 503.
[22] R. Gatignol, Théorie Cinétique des Gazes a Repartition Discrète de Vitesses. Lecture Notes in Physics, vol. 36, Springer-Verlag, Berlin, Germany, 1975.
[23] R. Monaco, L. Preziosi, Fluid dynamic applications of the discrete Boltzmann equations. Advances in Mathematics for Applied Sciences, vol. 3, World Scientific, Teaneck, 1991.
[24] J. Taylor, Lattice Boltzmann Model for Gasdynamics, Senior Thesis, Department of Physics, Santa Clara University, Santa Clara, 2001.
[25] P.L. Bhatnagar, E.P. Gross, M. Krook, A model for collision processes in gases I, Phys. Rev. 94 (1954) 511.
[26] A.J.C. Ladd, Numerical simulations of particulate suspensions via a discretized Boltzmann equation. Part 1. Theoretical foundation, J. Fluid Mech. 271 (1994) 285.
[27] Y.H. Qian, D. d'Humières, P. Lallemand, Lattice BGK model for Navier–Stokes equation, Europhys. Lett. 17 (1992) 479.
[28] J.D. Sterling, S. Chen, Stability analysis of lattice Boltzmann methods, J. Comput. Phys. 123 (1996) 196.

[29] X. He, S. Chen, G.D. Doolen, A novel thermal model for the lattice Boltzmann method in incompressible limit, J. Comput. Phys. 146 (1998) 282.
[30] B.J. Palmer, D.R. Rector, Lattice Boltzmann algorithm for simulating thermal flow in compressible fluids, J. Comput. Phys. 161 (2000) 1.
[31] F.J. Alexander, S. Chen, J.D. Sterling, Lattice Boltzmann thermohydrodynamics, Phys. Rev. E 47 (1993) R2249.
[32] S. Succi, I.V. Karlin, H. Chen, Colloquium: role of the H theorem in lattice Boltzmann hydrodynamic simulations, Rev. Mod. Phys. 74 (2002) 1203.
[33] F.J. Higuera, S. Succi, R. Benzi, Lattice gas dynamics with enhanced collisions, Europhys. Lett. 9 (1989) 345.
[34] H. Chen, S. Kandasamy, S. Orszag, R. Shock, S. Succi, V. Yakhot, Extended Boltzmann kinetic equation for turbulent flows, Science 301 (2003) 633.
[35] S. Succi, The Lattice Boltzmann Equation for Fluid Dynamics and Beyond, Oxford University Press, Oxford, UK, 2001.
[36] R. Benzi, S. Succi, M. Vergassola, The lattice Boltzmann equation–theory and applications, Phys. Rep. 222 (1992) 145.
[37] S. Chen, G.D. Doolen, Lattice Boltzmann method for fluid flow, Ann. Rev. Fluid. Mech. 30 (1998) 329.
[38] R. Courant, D. Hilbert, Methods of Mathematical Physics, vol. II, Interscience, New York, 1962.
[39] A. Arakawa, Computational design for long-term numerical integrations of the equations of atmospheric motion, J. Comput. Phys. 1 (1966) 119.
[40] J. Adams, P. Swarztrauber, R. Sweet, FISHPAK: A Package of Fortran Subroutines for the Solution of Separable Elliptic Partial Differential Equations, National Center for Atmospheric Research, Boulder, 1988. Available from http://www.scd.ncar.ucar.edu/softlib/FISHPAK.html
[41] B.P. Leonard, Elliptic systems: finite-difference method IV, in: J.W. Minkowycz, E.M. Sparrow, G.E. Schneider, R.H. Pletcher (Eds.), Handbook of Numerical Heat Transfer, Wiley, New York, 1988.